ARTICLE

Lanthanide Functionalized Covalent Triazine Framework as Physiological Molecular Thermometer

Received 00th January 20xx,
Accepted 00th January 20xx

DOI: 10.1039/x0xx00000x

Parviz Gohari Derakhshandeh,[a†] Sara Abednatanzi,[a†] Laurens Bourda,[a] Sasanka Dalapati,[ab] Anatolii Abalymov,[c] Maria Meledina,[de] Ying-Ya Liu,[f] Andre G. Skirtach,[c] Kristof Van Hecke,[a] Anna M. Kaczmarek* [a] and Pascal Van Der Voort *[a]

Crystalline covalent triazine frameworks (CTFs) with intrinsic porosity and high stability are excellent platforms for engineering luminescence properties, as their building blocks and guest ions are all potential actors in light emission. Herein, a highly crystalline bipyridine-based CTF (Bipy-CTF) is synthesized in mild conditions. The controlled tethering of lanthanide ions (Ln = Eu^{3+} and Tb^{3+}) onto Bipy-CTF combined with a selective photoexcitation results in a ratiometric luminescent thermometer (LnCTF). This LnCTF thermometer exhibits an excellent linear response in the solid state over a wide range of temperatures (200 to 340 K), with a temperature uncertainty below 0.2% and a very good reusability (up to 98.5% repeatability). Moreover, the suspended material in water shows a temperature sensitivity down to 253 K (– 20 °C), which is a very important finding for monitoring the physiological processes within biological and biochemical systems during freezing/defrosting treatment with precise temperature measurements. We also studied and confirmed the low cytotoxicity of the LnCTF towards cells opening prospects for future *in vivo* applications. This work thus highlights a new application of LnCTF materials as ratiometric luminescent molecular thermometers with excellent sensitivity in the physiological temperature range.

Introduction

Covalent organic frameworks (COFs) can be described as crystalline, ordered and porous organic polymers. They have a huge potential due to their crystalline structure, high porosity, and structural diversity.[1, 2] COFs have been designed for diverse applications including gas adsorption and separation, luminescence and sensing, catalysis, optoelectronics, drug delivery, water purification, CO_2 capture, energy storage and energy conversion.[3-14] Covalent triazine frameworks (CTFs), identified by their typical aromatic triazine linkages were reported for the first time in 2008 by Thomas and Antonietti.[15] They form a subclass of COFs and are especially interesting because of their high surface area, high nitrogen content and high physicochemical and thermal stability.[16, 17] Current strategies to design crystalline COFs involve reversible covalent bond formation, referred to as the "error-correcting" reversible bond formation approach. On the downside, COFs synthesized by highly reversible bond formations often show a poor stability. While COFs based on an imine linkage (C=N) are more robust than those with B-O bonds, they still suffer hydrolysis under acidic conditions.[18, 19] CTFs, on the other hand, form highly conjugated and stable materials, but often show moderate to poor crystallinity.

Up to date, a variety of approaches has been reported for the preparation of CTFs, such as the cyclization of nitrile or amide aromatic building blocks, using $ZnCl_2$ (ionothermal), P_2O_5 (ionothermal), CF_3SO_3H and $AlCl_3$ as catalysts.[15, 20-23] However, the high temperature (400-500 °C) of the ionothermal synthetic pathways leads to non-photoactive materials due to a partial carbonization. On the other hand, the other two catalytic pathways using triflic acid or $AlCl_3$ only show good results for a limited number of building blocks and amorphous materials are typically obtained. Recently, Cooper *et al.* developed a novel synthesis strategy involving the condensation reaction of aldehydes and amidines to make CTFs under relatively mild conditions.[24] This method provides a great opportunity to design novel porous structures using a variety of building blocks.[25-29] The resulting materials are typically obtained as yellow or orange powders, retaining most of their photophysical properties, while still not being crystalline. Tan *et al.* found that slowing down the nucleation process through in situ oxidation of alcohol monomers into aldehydes during the polycondensation reaction results in highly crystalline CTFs.[30] By introducing metal coordination sites, such as in the case of 2,2'-

[a.] *Department of Chemistry, Ghent University, Krijgslaan 281-S3, Ghent 9000, Belgium*
[b.] *Department of Materials Science, School of Technology, Central University of Tamil Nadu (CUTN), Thiruvarur-610005, Tamil Nadu, India.*
[c.] *Department of Biotechnology, Faculty of Bioscience Engineering, Ghent University Ghent 9000, Belgium.*
[d.] *RWTH Aachen University, Central Facility for Electron Microscopy, D-52074, Aachen, Germany*
[e.] *Forschungszentrum Jülich GmbH, Ernst Ruska-Centre (ER-C 2), D-52425, Jülich, Germany.*
[f.] *State Key Laboratory of Fine Chemicals, Dalian University of Technology, 116024, Dalian, PR China*
† These authors contributed equally to this work.
Electronic Supplementary Information (ESI) available: [details of any supplementary information available should be included here]. See DOI: 10.1039/x0xx00000x

bipyridine-based CTF (Bipy-CTF), metal complexes can be tethered onto the CTFs. Such materials have already shown great results in heterogeneous catalysis.[31] Clearly, also photoactive CTFs can be synthesized in this way.

Temperature is a fundamental thermodynamic parameter, the measurement of which is crucial in both science and industrial applications. Generally, traditional thermometers such as thermistors, thermocouples and liquid-filled thermometers are not applicable at the submicrometer scale. Therefore, precise temperature measurement is still challenging in the fields of nanotechnology and nanomedicine, but it is essential for biomedical applications, for example intracellular release.[32] This has encouraged scientists to develop new temperature sensors to measure temperature with micrometric and nanometric precision. Luminescent thermometers are of great interest due to their brilliant color visibility and temperature-dependent luminescence features. High sensitivity, instant response, noninvasive functioning and applicability in strong magnetic or electric fields are some of the important benefits of luminescent thermometers compared to other molecular thermometers. The trivalent lanthanides (Ln^{3+}) have attracted comprehensive attention and are often used in luminescence due to their unique spectroscopic characteristics, particularly, narrow band emission, long lifetime, and high quantum yield values.

The integration of lanthanide ions or complexes with organic bridging linkers is a well-studied methodology to overcome the low absorption coefficients of lanthanides. We and others have prepared lanthanide tethered metal-organic frameworks (MOFs), coordination polymers (CPs) and periodic mesoporous organosilicas (PMOs).[33-40] Still, some of these materials such as LnMOFs and CPs suffer from low stability and low water dispersibility and are cytotoxic. As COFs have a very low biological toxicity[41, 42], the immobilization of lanthanide (Ln) ions onto COFs can result in excellent temperature sensors arising from their multiple luminescence centers and highly tunable luminescence properties.[43-45] However, most of the COFs are non-luminescent, because of non-radiative deactivation arising from intramolecular bond rotation and aggregation-caused quenching (ACQ) driven by the π-π stacking in the structure. In this regard, the confinement of intramolecular bond rotation and/or the construction of relatively rigid frameworks is one approach to enhance the photoluminescence activity by minimizing non-radiative deactivation. This is the main reason that we targeted CTFs, as they have a rigid framework built by triazine linkages and show minimal intramolecular rotation by 'exocyclic' covalent bonds. Besides, the organic donor-acceptor pairs and crystalline structure of the Bipy-CTF greatly improve the delocalization of π electrons to overcome ACQ. These features make Bipy-CTF an excellent candidate for photoluminescent applications.[18, 19]

In this work, we present a novel application of CTFs as photoluminescent materials. For this purpose, we designed a bipyridine-based CTF via the polycondensation reaction of Bipy containing monomers and 1,4-benzenedimethanol. The nitrogen-rich material provides excellent docking sites for immobilization of various guests, examined for two different lanthanide guests (Eu^{3+} and Tb^{3+}). The Bipy sites not only act as anchoring points for lanthanides but also enable the excitation of Ln^{3+} ions through intramolecular energy transfer known as the "antenna effect". The obtained materials exhibit excellent temperature sensing properties in the physiological range. The Bipy-CTF before and after immobilization with lanthanides showed low cytotoxicity to human fibroblastic cells even at high concentration and showed excellent temperature sensing properties, also in water. To the best of our knowledge, this is the first report on the applicability of LnCTFs as photoluminescent materials for physiological molecular thermometers.

Experimental Section

Synthesis of 2,2'-bipyridine-5,5'-diamidine dihydrochloride: To a solution of 2,2'-bipyridine-5,5'-dicarbonitrile (0.412 g, 2.0 mmol) in 8 mL THF, 8 mL of 1 M $LiN(SiMe_3)_2$ solution was added dropwise over the time of 30 min at 0 °C. The mixture was stirred at 25 °C for 24 h and then cooled to 0 °C. The reaction was quenched by careful addition of 6 M HCl–EtOH (8 mL) and the mixture was left overnight. The solid sample was then filtered and washed with diethyl ether. Hereafter, the solid was recrystallized from H_2O–EtOH mixture. Yield: (0.767 g, 96%). 1H NMR (400MHz, DMSO-d6): δ = 9.80 (s, 4H, NH), 9.53 (s, 4H, NH), 9.18 (d, 2H, aromatic H), 8.63 (d, 2H, aromatic H), 8.47 (d, 2H, aromatic H), 13C NMR (75 MHz, D2O) δ = 164.36, 158.19, 148.30, 138.15, 125.65, 122.81.

Synthesis of Bipy-CTF: 1,4-Benzenedimethanol (0.069 mg, 0.5 mmol), 2,2'-bipyridine-5,5'-diamidine dihydrochloride (0.311 g, 1.0 mmol), and cesium carbonate (0.700 g, 2.2 mmol) were added to a DMSO solution (15.0 mL) in a round-bottom flask (100 mL). The mixture was heated at 100 °C for 24 h, then the temperature was raised to 150 °C for 36 h. The precipitates of the yellow suspension was washed with diluted HCl (1M, 3 × 20 mL) to remove residual cesium carbonate, and further washed with water (3 × 30 mL), EtOH (3 × 30 mL), and THF (3 × 20 mL). The filtered solids were freeze-dried for 24 h to yield Bipy-CTF as a yellow power (150 mg, 84% yield).

Synthesis of Ln@Bipy-CTF: The samples were prepared by weighting of 0.005 mmol of the Bipy-CTF and 0.005 mmol of $Ln(bzac)_3{\cdot}2H_2O$ (bzac = benzoylacetone) complexes and both powders were placed it in a Pyrex tube. After the addition of dichloromethane (5 mL), the sealed tube was placed in an ultrasound bath for 10 minutes. Then, the tube was heated on a heating block at 45 °C for 24 h. Afterwards, the filtered powder was washed with tiny amount of methanol and dried at 80 °C.

Results and Discussion

The Bipy-CTF material was synthesized by condensation of 2,2'-bipyridine-5,5'-diamidine dihydrochloride with 1,4 benzenedimethanol (Figure 1A and 1B). The successful formation of the triazine frameworks was confirmed by diffuse reflectance infrared Fourier transform spectroscopy (DRIFTS)

ARTICLE

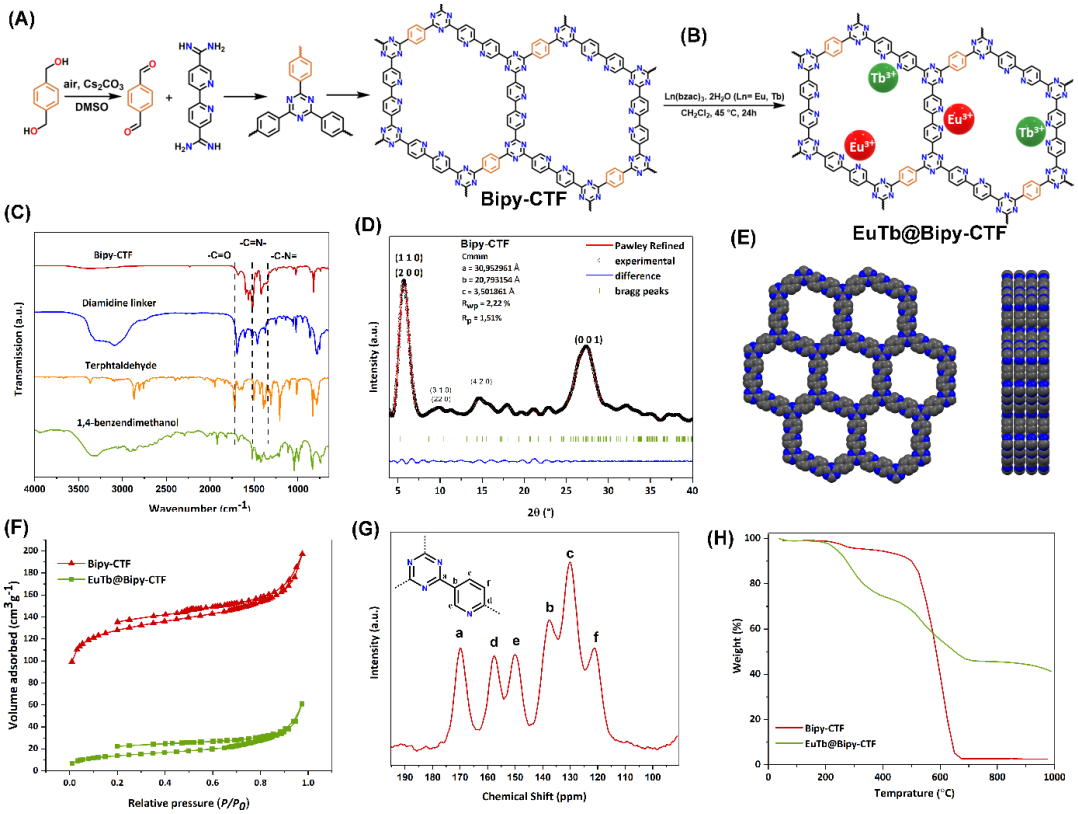

Figure 1. A) Scheme showing the triazine framework synthesis through in situ formation of aldehyde monomers by controlled oxidation of alcohol monomers and condensation with amidine, and B) LnCTF (Ln = Eu,Tb) synthesis. C) DRIFTS of Bipy-CTF, diamidine linker, terephtaldehyde and 1,4-benzendimethanol. D) Background corrected experimental (black) and Pawley refined (red) PXRD patterns of Bipy-CTF AA stacking, accompanied with the difference plot (blue) and Bragg peak positions (green) of the model. E) Top and side views of the Bipy-CTF structure, carbon is shown in grey, nitrogen in blue, hydrogens were omitted for clarity. F) Nitrogen (N_2) adsorption/desorption isotherms of Bipy-CTF (black) and EuTb@Bipy-CTF (red). G) Solid-state 13C CP/MAS NMR spectra of Bipy-CTF. H) TGA data of Bipy-CTF (black) and EuTb@Bipy-CTF (red) measured under air atmosphere.

analysis, revealing the characteristic stretching vibrations from the triazine units at ~1516 and 1351 cm^{-1} for Bipy-CTF (Figure 1 C). Also, the disappearance of the intense aldehyde band (~1716 cm^{-1}) and broad O-H band (~3300 cm^{-1}) is indicative of the complete consumption of the monomers to form triazine linkages. The carbon and nitrogen contents obtained from elemental analysis are in close agreement to the theoretical values (Table S1).

The experimental and simulated structural X-ray diffraction (XRD) patterns of Bipy-CTF are shown in Figure 1D and 1E. Powder XRD was used to characterize the crystalline nature of the synthesized material. Bipy-CTF exhibits two major peaks, one is centered at 5.5°, which is assigned to the combination of the (110) and (200) reflection and a broad peak at 26.8°, indicative for the d-spacing between layers or (001) reflection. Some smaller peaks matching with predicted Bragg peaks could also be observed in the background corrected pattern, namely the combined (310) and (220) reflections centered at 9.9° and the (420) reflection at 14.6°. For the Bipy-CTF the eclipsed (AA) and staggered (AB) structures were compared (Figure 1D and S14). The eclipsed stacking structure matches best with the theoretical XRD pattern and with the experimental pattern. Subsequently, Pawley refinements were carried out for the eclipsed structure of Bipy-CTF and an optimized structure assigned to the *Cmmm* space group with unit cell parameters of a = 30.95 Å, b = 20.79 Å and c = 3.50 Å with a refined parameter of R_p =1.51% and wR_p = 2.22%. The diffractograms point at a

good crystallinity for the Bipy-CTF material, rarely observed for the previously reported CTFs.

The porosity of the Bipy-CTF was determined by N_2 sorption measurements at 77 K. As shown in Figure 1F, the Bipy-CTF displayed typical type I isotherm, indicative for a microporous material. The Bipy-CTF exhibited Brunauer–Emmett–Teller (BET) and Langmuir surface area of 439 and 635 m^2g^{-1}, respectively. The total pore volume is 0.23 cm^3g^{-1} at $P/P_0 = 0.98$. As shown in Figure 1G, the ^{13}C CP/MAS solid-state NMR spectrum of Bipy-CTF exhibits five well-resolved signals at 121, 130, 137.5, 149.9, and 157.5 ppm, which can be assigned to the Bipy carbons. Furthermore, the appearance of a peak at 169.8 ppm is characteristic of the carbon signal from triazine rings which clearly confirms the formation of triazine units in the Bipy-CTF.[24, 30] The thermogravimetric analysis (TGA) reveals excellent thermal stability of the Bipy-CTF material with no weight loss up to ~600 °C (Figure 1H). Furthermore, scanning electron microscopy (SEM) shows micrometer-sized particles with no particular shape (Figure S1). Transmission electron microscopic (TEM) and high resolution (HR)-TEM images were taken to further investigate the microscopic structures analysis of the Bipy-CTF. The layered and crystalline structure of Bipy-CTF with ordered lattice structure is visible in ADF-STEM and HR-TEM images (Figure 2a and S2).

As mentioned above, the key to resolve the limitations of photoluminescent materials lies in the development of crystalline porous material with limited intramolecular rotation and delocalized π electrons system while the stability is still preserved. Accordingly, the crystalline, stable, porous Bipy-CTF material was applied to examine its potential application as luminescent molecular thermometer in the physiological temperature range. The Bipy-CTF material comprises numerous N functionalities, including triazine and bipyridine edges that form ideal docking sites for grafting of Eu^{3+} and Tb^{3+} complexes simultaneously *via* a post-modification procedure (Figure 1B). The immobilization of Eu^{3+} and Tb^{3+} complexes on the Bipy-CTF was confirmed by DRIFTS analysis (Figure S3). In the DRIFTS spectra of the Eu,Tb@Bipy-CTF sample, the existence of intense bands at 1599 cm^{-1} (C=O) and 1569 cm^{-1} (C=C) is observed, which is attributed to the presence of lanthanide complexes in the framework. Moreover, the bands around 2850-3060 cm^{-1} are related to ν(C-H) and also present in the EuTb@Bipy-CTF sample. Additionally, because of its coordination to the lanthanides, the C=N peak of the bipyridine linker shifts from 1685 to 1675 cm^{-1} in the EuTb@Bipy-CTF. In addition, the overall N_2 uptake of EuTb@Bipy-CTF decreased upon grafting, indicating the successful immobilization of lanthanides within the porous channel of CTF framework (Figure 1F). The BET and Langmuir surface area of Eu,Tb@Bipy-CTF decreased notably to 50 and 89 m^2g^{-1}, respectively, and the total pore volume reduced to 0.06 $cm^3\ g^{-1}$. The crystallinity of the hosting network is also clearly visualized by means of ADF-STEM (Figure 2b). TEM-EDX analysis of LnCTF was carried out to check the presence of the Eu and Tb elements in the Bipy-CTF after post-modification (Figures S4). The observed results reveled that both Eu and Tb ions are well distributed within the EuTb@Bipy-CTF skeletons. The optical absorption property of the yellowish pristine Bipy-CTF sample was measured by Diffuse Reflectance (DR)-UV-visible spectrophotometry. It was observed that the material could absorb a wide range of visible light (Figure S5). The luminescence properties of the pristine Bipy-CTF were first investigated at room temperature (Figure S6). Upon excitation with UV light, the Bipy-CTF shows broad emission in the range of 450 - 750 nm, with a peak maximum centered at 575 nm. The luminescence properties of the materials were also studied after grafting with lanthanide complexes. Figure 3A demonstrates a picture of the four samples, Tb@Bipy-CTF (**1**),

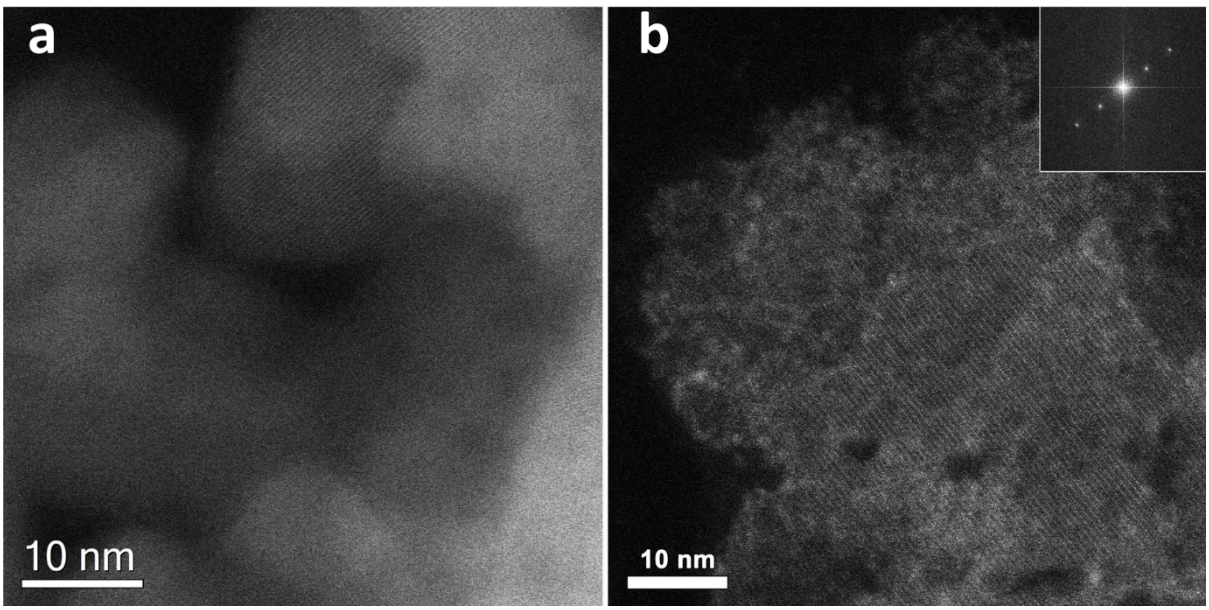

Figure 2. ADF-STEM image of a) pristine Bipy-CTF b) Bipy-CTF after loading together with corresponding FFT in the inset revealing the crystallinity of the materials.

Eu@Bipy-CTF (**2**), 3%Eu,97%Tb@Bipy-CTF (**3**) and 5%Eu,95%Tb@Bipy-CTF (**4**) upon exposing to a UV lamp at 302 nm excitation wavelength. It can be observed that the emitted colors are green, red and yellow respectively (with different yellow undertones).

All four compounds show strong visible emission with the characteristic f-f transitions of the lanthanides upon exciting into the maximum of the broad linker band originating from the pristine CTF (250 - 400 nm) (Figure 3). The labelled peaks in the spectra are assigned in the SI (Table S2-S5). The decay times of the compounds are also presented in the SI (Figures S7-S9 and table S6). In addition, we studied the temperature dependence luminescence characteristics of two Eu-Tb co-doped compounds, as it is known that this lanthanide pair can be used for developing optical thermometers. Ratiometric thermometers are thermometers based on the intensity (wavelength) ratio of two transitions (Eu^{3+} and Tb^{3+} in this case) that suffer from certain limtations such as fluctuations of the excitation source. Here, the emission spectra of the samples were measured at various temperatures, from 200 – 340 K (Figure 4).

For compound **3** the I_{549}/I_{610} ratio of the integrated areas was calculated (Tb^{3+}: 530 – 565; Eu^{3+}: 605-630) for the 200 - 340 K temperature range (Figure 4A). The obtained data points could be fitted excellently using the equation for Δ (R^2 = 0.996) yielding ΔE = 1203 cm^{-1} (Figure 4B). The nonradiative deactivation energies might be involved the ligand triplet level and the $^5D_4$ level of Tb^{3+} (the triplet level of the Bipy-CTF has been determined and is presented in the Figures S10-S11). Figure 4B represents the plot that shows the calibration curve. The maximum number of the relative temperature sensitivity, Sr was determined to be 2.30% K^{-1} (240 K) (Figure 4C). For compound **4** also, the I_{549}/I_{610} ratio of the integrated areas was calculated (Tb^{3+}: 530 – 565; Eu^{3+}: 605-630). The emission map recorded at different temperatures (253 – 333 K) is presented in Figure 4D. These data points could be well fitted employing the equation for Δ (R^2 = 0.985) yielding ΔE = 948 cm^{-1} (Figure 4E). Also, in the case of this material the nonradiative deactivation energies probably involve the ligand triplet level and the $^5D_4$ level of Tb^{3+}. The plot, showing the calibration curve, is presented in Figure 4E. The maximum value of Sr was determined to be 2.12% K^{-1} (253 K) (Figure 4F). A schematic representation of the energy levels of the Tb^{3+}, Eu^{3+} and the singlet and triplet levels of ligands along with the possible ways of energy transfer from Tb^{3+} to Eu^{3+} is given in Scheme S1. Both materials

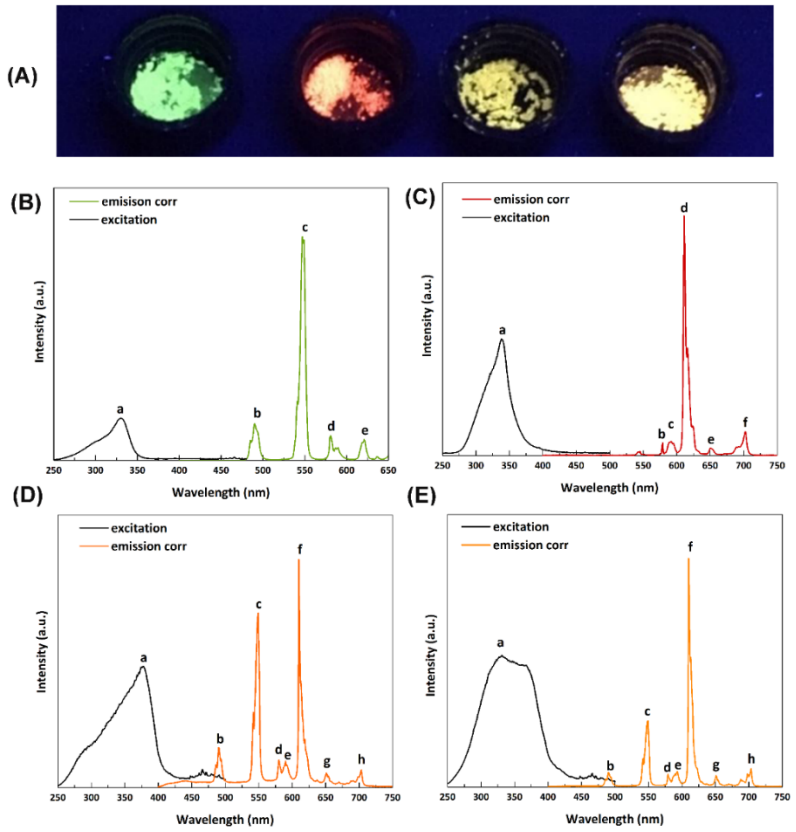

Figure 3. A) Photo taken whenplacing **1**, **2**, **3** and **4** (from left to right) samples under a UV lamp (302 nm excitation). Combined excitation-emission spectra of B) **1**, C) **2**, D) **3** and E) **4** compounds. The labeled peaks have been assigned in the SI (Table S2-S5).

ARTICLE

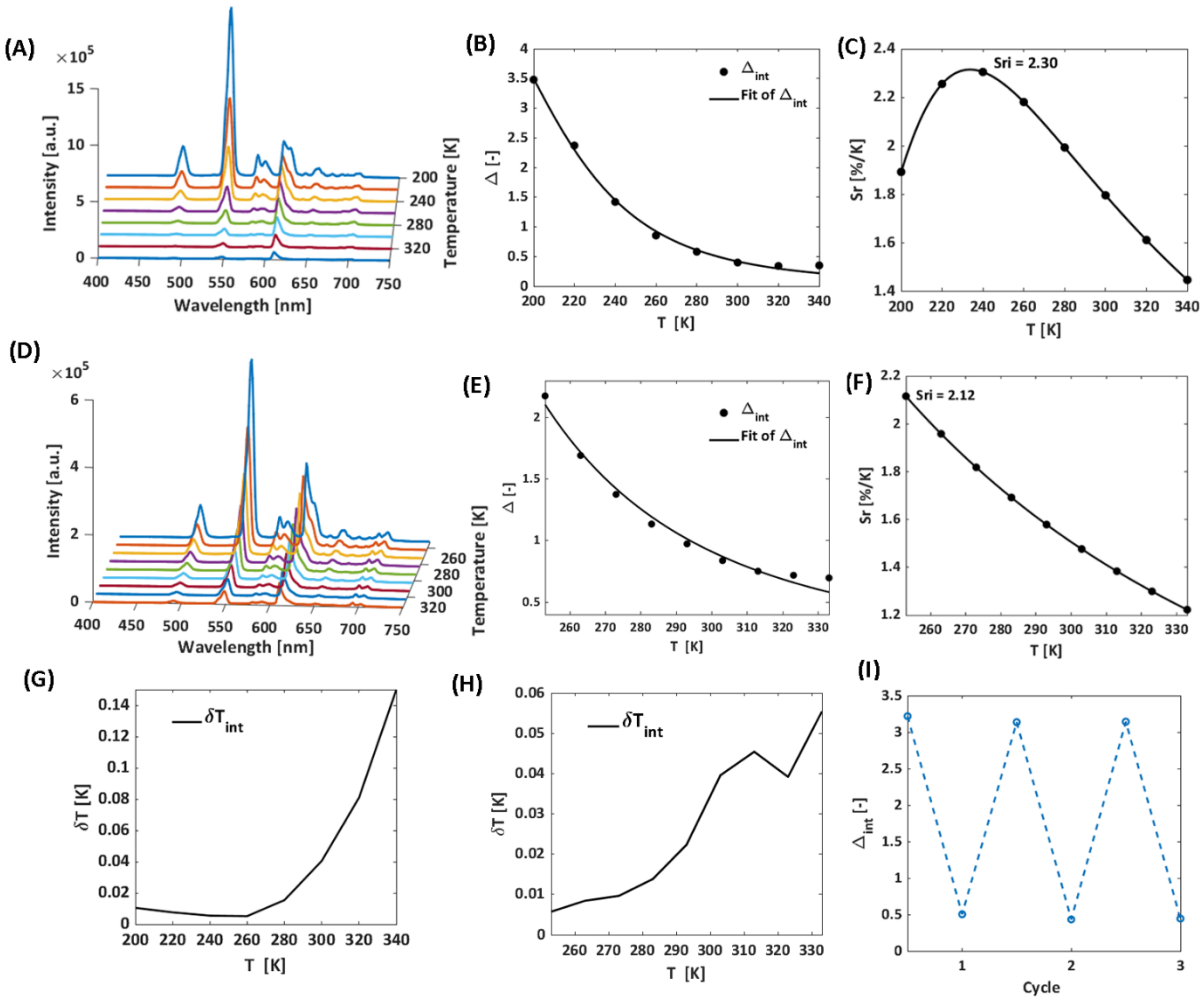

Figure 4. A) Emission map of **3** recorded between 200-340 K with a step size of 20K. B) Plot presenting the calibration curve of **3** when the equation for Δ is employed. The points show the experimental delta parameters and the solid like presents the best fit of the experimental points. C) Plot presenting the relative sensitivity Sr values at varied temperatures (200-340 K) for compound **3**. D) Emission map of **4** recorded between 253-333 K with a step size of 10K. E) Plot presenting the calibration curve of **4** when the equation for Δ is employed. The points show the experimental delta parameters and the solid like presents the best fit of the experimental points; F) Plot presenting the relative temperature sensitivity Sr values at varied temperatures (253-333 K) for compound **4**. The solid line is a guide to increase visibility. G) Graph presenting the temperature uncertainty for compound **3** and H) compound **4**. I) Cycle test showing reusability of the compound **3** thermometer material (98.5% repeatability).

Show good thermometric performance in the extended physiological range compared to the previous reports (Table S7). For both compounds the uncertainty was calculated and was determined to be very low, below 0.2%, which means these thermometers show very good performance in the solid state (Figure 5G, H). To additionally prove that they can be reused for several measurement runs the compound **3** was tested for its recyclability. It showed up to 98.5% repeatability (Figure 5I).

Inspired by the good performance of the LnCTF thermometers in the physiological temperature range, we further investigated their performance in water. Moreover, we performed cytotoxicity tests on human cells. The sample **3** was also selected for studying the thermometric properties in water. For the temperature-dependent luminescence measurements, a suspension was prepared by adding 1 mg of the sample in 1 mL of distilled water. The suspension demonstrated a light red

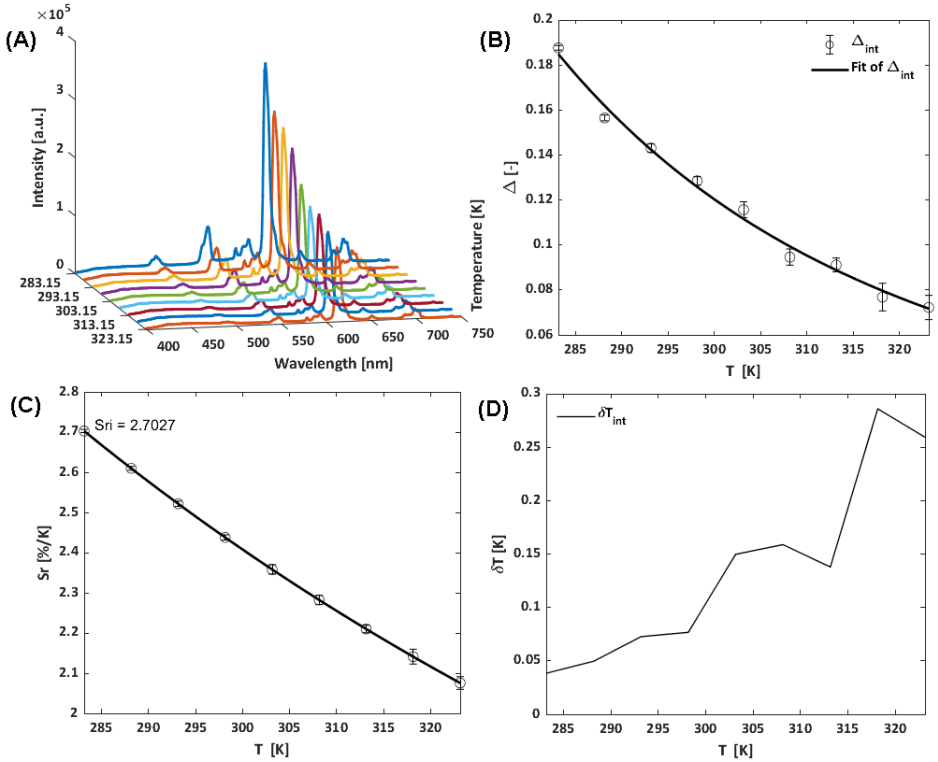

Figure 5. A) Emission map of sample **3** recorded between 283.15-323.15 K with a step size of 5 K in a water suspension. B) Plot presenting the calibration curve of compound **3** when the equation for Δ is employed. The points show the experimental delta parameters and the solid like presents the best fit of the experimental points. C) Plot presenting the relative sensitivity Sr values at varied temperatures (283.15-323.15 K) for compound **3** in water suspension. D) Graph presenting the temperature uncertainty for **3** measured in water suspension.

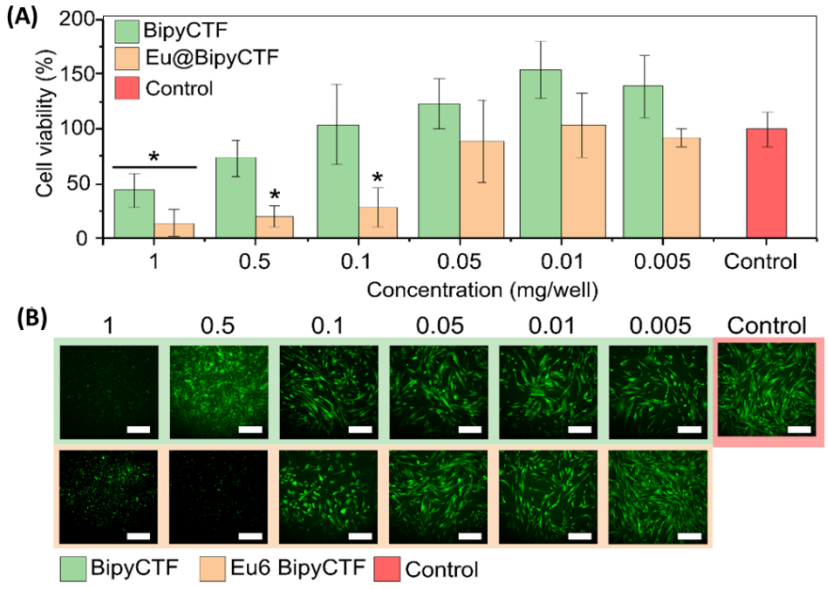

Figure 6. A) Graph presenting the cell viability (%) after exposure to different concentrations of the BipyCTF and compound **2** particles. An asterisk (*) indicates significant differences from the control cell group. The statistical analysis was performed by ANOVA followed by the Tukey test ($p < 0.05$). B) Fluorescence microscopy images of the cells at different compound concentrations (cells are green). Scale bar is 250 µm.

emission color when illuminated by a UV lamp (302 nm). The thermometric properties of the Eu,Tb@Bipy-CTF compound were measured over 283.15 - 323.15 K, with a step size of 5 K. The emission map of the material is presented in Figure 5A. The data points are well fitted by using the equation for Δ (R^2 = 0.992) giving ΔE = 1506 cm^{-1} (Figure 5B). The maximum relative sensitivity Sr was calculated to be 2.70 % K^{-1} (283.15 K) (Figure 5C). Due to the stronger influence of signal-to-noise ratio in the measurements performed in water, we have included error bars on the plots of Delta and Sr. This result is somewhat higher than that reported for powder samples. This can be explained by the fact that the sample is solvatochromic and in water the ratio of Tb-to-Eu may change compared to the powder, which influences the final thermometric performance of the material. The temperature uncertainty δT has been plotted in Figure 5D. The increase in δT is due to a weaker signal of the material when measured in water compared to solid state. However at maximum, it only reaches up to 0.3 K, which is a very good value. This additional dataset indicates that the lanthanide-grafted CTF materials show good performance in colloidal water suspension, confirming its potential application as biological thermometers.

To fully evaluate the suitability of these materials for employing in biomedical systems, it is essential to investigate their cytotoxicity towards living cells. Accordingly, we carried out experiments using normal human dermal fibroblastic cells (NHDF cells). The viability tests of the cells demonstrated that the Bipy-CTF and Ln@Bipy-CTF materials are non-toxic at lower concentrations (Figure 6A). The particle toxicity towards fibroblastic cells occurred only at very high concentrations of 1 and 0.5 mg per well for Bipy-CTF and Ln@Bipy-CTF, respectively, that might be due to the mechanical pressure of the particles on the cells. The fluorescence images show the morphology of cells after incubation with the particles (Figure 6B). The fusiform morphology of cells incubated with Bipy-CTF and Ln@BipyCTF at 0.1 mg/ml and lower concentrations are comparable to control which fully correlates with the cell viability test. High stability, very good thermometric performance in solid-state and water and, nontoxicity to human cells make these compounds very promising to be used in the biological systems.

Conclusions

Here, we report the synthesis of a new bipyridine-based CTF, where the bipyridine linker was purposefully introduced for the selective docking of lanthanide ions. We successfully synthesized a highly crystalline, porous and robust Bipy-CTF *via* in situ generation of an aldehyde intermediate. We applied a polycondensation strategy by using a simple bipyridine amidine monomer, which opens immense possibilities of monomers design for synthesizing new crystalline CTFs under mild conditions. The organic donor-acceptor pairs and ordered structure of the conjugated Bipy-CTF moiety greatly improve the delocalization of π electrons to overcome nonradiative energy dissipation. With these collective advantages of crystalline and porous Bipy-CTF in hand, docking various lanthanide ions not only enable luminescence color tuning but also facilitating the excitation of lanthanide ions through antenna effect. The presence of bipyridine docking sites within the porous channel-wall of the Bipy-CTF allows an easy and controlled grafting of lanthanide complexes, which open up a new avenue for designing LnCTF based ratiometric luminescent thermometers. The EuTb@Bipy-CTF thermometer exhibited excellent linear response over wide range of temperature from 200 to 340 K, with a temperature uncertainty below 0.2% and very good reusability (up to 98.5% repeatability). Moreover, the thermometer also exhibited excellent performance in the physiological temperature range when dispersed in water. High crystallinity and stability, outstanding thermometric performance in the solid-state as well as in water and nontoxicity to human fibroblastic cells make this LnCTF material a very promising candidate as physiological molecular thermometer.

Author contributions

P. Gohari Derakhshandeh: Investigation, Writing – original draft, Formal analysis. S. Abednatanzi: Investigation, Writing – original draft, Formal analysis. L. Bourda: Formal analysis. S. Dalapati: Conceptualization, Writing – review & editing. A. Abalymov: Investigation. M. Meledina: Formal analysis. Y.-Ya Liu: Formal analysis. A. G. Skirtach: Resources, Supervision. K. Van Hecke: Validation, Supervision. A. M. Kaczmarek: Conceptualization, Supervision, Writing – review & editing. P. Van Der Voort: Conceptualization, Supervision, Resources, Writing – review & editing.

Conflicts of interest

There are no conflicts to declare.

Acknowledgements

PGD and SA gratefully acknowledge the financial support from the Research Foundation Flanders (FWO Vlaanderen) grant No. G000117N. SA acknowledges the financial support from the Ghent University BOF doctoral grant 01D04318. SD would like to acknowledge “European Union’s Horizon 2020 research and innovation programme under the Marie Sklodowska-Curie grant agreement No. 840011” for funding support. AGS acknowledges support of FWO Flanders (I002620N, G043219) and BOF UGent (01IO3618, BAS094-18). Y.-Y. L. would like to thank International S&T Cooperation Program of China (2016YFE0109800). M.M. wants to acknowledge the Verbundvorhaben iNEW: Inkubator Nachhaltige Elektrochemische Wertschöpfungsketten with the funding number 03SF0589A (German Federal Ministry for Economic Affairs and Energy BMWi). KVH thanks the Special Research Fund (BOF) – UGent (project 01N03217) for funding. AA thanks the support of the program “Global Education”. A.M.K. would like to thank Ghent University for BOF funding (BOF/STA/202002/004). The authors thank Mr. Olivier Janssens for SEM measurements.

Notes and references

1. C. S. Diercks and O. M. Yaghi, *Science*, 2017, **355**.
2. S. Kandambeth, K. Dey and R. Banerjee, *J Am Chem Soc*, 2019, **141**, 1807-1822.
3. X. Zhu, C. C. Tian, G. M. Veith, C. W. Abney, J. Dehaudt and S. Dai, *J Am Chem Soc*, 2016, **138**, 11497-11500.
4. S. Abednatanzi, P. G. Derakhshandeh, K. Leus, H. Vrielinck, F. Callens, J. Schmidt, A. Savateev and P. V. D. Voort, *Sci. Adv.*, 2020, **6**, eaaz2310.
5. X. Y. Wang, L. J. Chen, S. Y. Chong, M. A. Little, Y. Z. Wu, W. H. Zhu, R. Clowes, Y. Yan, M. A. Zwijnenburg, R. S. Sprick and A. I. Cooper, *Nat Chem*, 2018, **10**, 1180-1189.
6. S. M. J. Rogge, A. Bavykina, J. Hajek, H. Garcia, A. I. Olivos-Suarez, A. Sepulveda-Escribano, A. Vimont, G. Clet, P. Bazin, F. Kapteijn, M. Daturi, E. V. Ramos-Fernandez, F. X. L. I. Xamena, V. Van Speybroeck and J. Gascon, *Chem Soc Rev*, 2017, **46**, 3134-3184.
7. X. Y. Guan, F. Q. Chen, Q. R. Fang and S. L. Qiu, *Chem Soc Rev*, 2020, **49**, 1357-1384.
8. Z. F. Wang, S. N. Zhang, Y. Chen, Z. J. Zhang and S. Q. Ma, *Chem Soc Rev*, 2020, **49**, 708-735.
9. X. G. Liu, D. L. Huang, C. Lai, G. M. Zeng, L. Qin, H. Wang, H. Yi, B. S. Li, S. Y. Liu, M. M. Zhang, R. Deng, Y. K. Fu, L. Li, W. J. Xue and S. Chen, *Chem Soc Rev*, 2019, **48**, 5266-5302.
10. M. Dogru and T. Bein, *Chem Commun*, 2014, **50**, 5531-5546.
11. A. K. Mandal, J. Mahmood and J. B. Baek, *Chemnanomat*, 2017, **3**, 373-391.
12. L. Ascherl, E. W. Evans, M. Hennemann, D. Di Nuzzo, A. G. Hufnagel, M. Beetz, R. H. Friend, T. Clark, T. Bein and F. Auras, *Nat Commun*, 2018, **9**.
13. S. Haldar, D. Chakraborty, B. Roy, G. Banappanavar, K. Rinku, D. Mullangi, P. Hazra, D. Kabra and R. Vaidhyanathan, *J Am Chem Soc*, 2018, **140**, 13367-13374.
14. A. Laemont, S. Abednatanzi, P. G. Derakshandeh, F. Verbruggen, E. Fiset, Q. Qin, K. Van Daele, M. Meledina, J. Schmidt, M. Oschatz, P. Van Der Voort, K. Rabaey, M. Antonietti, T. Breugetmans and K. Deus, *Green Chem*, 2020, **22**, 3095-3103.
15. P. Kuhn, M. Antonietti and A. Thomas, *Angew Chem Int Edit*, 2008, **47**, 3450-3453.
16. M. Y. Liu, L. P. Guo, S. B. Jin and B. E. Tan, *J Mater Chem A*, 2019, **7**, 5153-5172.
17. P. Puthiaraj, Y. R. Lee, S. Q. Zhang and W. S. Ahn, *J Mater Chem A*, 2016, **4**, 16288-16311.
18. K. Geng, T. He, R. Liu, S. Dalapati, K. T. Tan, Z. Li, S. Tao, Y. Gong, Q. Jiang and D. Jiang, *Chemical Reviews*, 2020, DOI: 10.1021/acs.chemrev.9b00550.
19. X. L. Li, C. L. Zhang, S. L. Cai, X. H. Lei, V. Altoe, F. Hong, J. J. Urban, J. Ciston, E. M. Chan and Y. Liu, *Nat Commun*, 2018, **9**.
20. S. H. Je, H. J. Kim, J. Kim, J. W. Choi and A. Coskun, *Adv Funct Mater*, 2017, **27**.
21. P. Puthiaraj, S. M. Cho, Y. R. Lee and W. S. Ahn, *J Mater Chem A*, 2015, **3**, 6792-6797.
22. S. J. Ren, M. J. Bojdys, R. Dawson, A. Laybourn, Y. Z. Khimyak, D. J. Adams and A. I. Cooper, *Adv Mater*, 2012, **24**, 2357-2361.
23. S. Y. Yu, J. Mahmood, H. J. Noh, J. M. Seo, S. M. Jung, S. H. Shin, Y. K. Im, I. Y. Jeon and J. B. Baek, *Angew Chem Int Edit*, 2018, **57**, 8438-8442.
24. K. W. Wang, L. M. Yang, X. Wang, L. P. Guo, G. Cheng, C. Zhang, S. B. Jin, B. Tan and A. Cooper, *Angew Chem Int Edit*, 2017, **56**, 14149-14153.
25. Y. Z. Tang, H. L. Huang, W. J. Xue, Y. J. Chang, Y. Li, X. Y. Guo and C. L. Zhong, *Chem Eng J*, 2020, **384**.
26. J. Li, P. Liu, Y. Z. Tang, H. L. Huang, H. Z. Cui, D. H. Mei and C. L. Zhong, *Acs Catal*, 2020, **10**, 2431-2442.
27. L. P. Guo, Y. L. Niu, H. T. Xu, Q. W. Li, S. Razzaque, Q. Huang, S. B. Jin and B. Tan, *J Mater Chem A*, 2018, **6**, 19775-19781.
28. Y. Jiang, I. Oh, S. H. Joo, O. Buyukcakir, X. Chen, S. H. Lee, M. Huang, W. K. Seong, J. H. Kim, J. U. Rohde, S. K. Kwak, J. W. Yoo and R. S. Ruoff, *Acs Nano*, 2019, **13**, 5251-5258.
29. L. P. Guo, Y. L. Niu, S. Razzaque, B. Tan and S. B. Jin, *Acs Catal*, 2019, **9**, 9438-9445.
30. M. Y. Liu, Q. Huang, S. L. Wang, Z. Y. Li, B. Y. Li, S. B. Jin and B. Tan, *Angew Chem Int Edit*, 2018, **57**, 11968-11972.
31. S. Abednatanzi, P. G. Derakhshandeh, P. Tack, F. Muniz-Miranda, Y.-Y. Liu, J. Everaert, M. Meledina, F. V. Bussche, L. Vincze, C. V. Stevens, V. V. Speybroeck, H. Vrielinck, F. Callens, K. Leus and P. V. D. Voort, *Applied Catalysis B: Environmental*, 2020, **269**, 118769.
32. A. G. Skirtach, A. M. Javier, O. Kreft, K. Kohler, A. P. Alberola, H. Mohwald, W. J. Parak and G. B. Sukhorukov, *Angew Chem Int Edit*, 2006, **45**, 4612-4617.
33. X. T. Rao, T. Song, J. K. Gao, Y. J. Cui, Y. Yang, C. D. Wu, B. L. Chen and G. D. Qian, *J Am Chem Soc*, 2013, **135**, 15559-15564.
34. Y. J. Cui, R. J. Song, J. C. Yu, M. Liu, Z. Q. Wang, C. D. Wu, Y. Yang, Z. Y. Wang, B. L. Chen and G. D. Qian, *Adv Mater*, 2015, **27**, 1420-+.
35. S. N. Zhao, L. J. Li, X. Z. Song, M. Zhu, Z. M. Hao, X. Meng, L. L. Wu, J. Feng, S. Y. Song, C. Wang and H. J. Zhang, *Adv Funct Mater*, 2015, **25**, 1463-1469.
36. Y. J. Cui, H. Xu, Y. F. Yue, Z. Y. Guo, J. C. Yu, Z. X. Chen, J. K. Gao, Y. Yang, G. D. Qian and B. L. Chen, *J Am Chem Soc*, 2012, **134**, 3979-3982.
37. A. M. Kaczmarek, Y. Maegawa, A. Abalymov, A. G. Skirtach, S. Inagaki and P. Van Der Voort, *Acs Appl Mater Inter*, 2020, **12**, 13540-13550.
38. P. G. Derakhshandeh, J. Soleimannejad, J. Janczak, A. M. Kaczmarek, K. Van Hecke and R. Van Deun, *Crystengcomm*, 2016, **18**, 6738-6747.
39. Y. F. Zhao and D. Li, *J Mater Chem C*, 2020, **8**, 12739-12754.
40. J. Q. Liu, X. Z. Yue, Z. P. Wang, X. Zhang and Y. Xu, *J Mater Chem C*, 2020, **8**, 13328-13335.
41. V. S. Vyas, M. Vishwakarma, I. Moudrakovski, F. Haase, G. Savasci, C. Ochsenfeld, J. P. Spatz and B. V. Lotsch, *Adv Mater*, 2016, **28**, 8749-8754.
42. P. Wang, F. Zhou, C. Zhang, S. Y. Yin, L. L. Teng, L. L. Chen, X. X. Hu, H. W. Liu, X. Yin and X. B. Zhang, *Chem Sci*, 2018, **9**, 8402-8408.
43. J. M. Wang, X. Lian and B. Yan, *Inorg Chem*, 2019, **58**, 9956-9963.
44. J. Li, C. Y. Zhang, M. Y. Yin, Z. Zhang, Y. J. Chen, L. Deng and S. Wang, *Acs Omega*, 2019, **4**, 15947-15955.
45. A. M. Kaczmarek, Y. Y. Liu, M. K. Kaczmarek, H. S. Liu, F. Artizzu, L. D. Carlos and P. Van Der Voort, *Angew Chem Int Edit*, 2020, **59**, 1932-1940.